The Zinc Binding Site of the *Shaker* Channel KDC1 from *Daucus carota*

Cristiana Picco, Alessia Naso, Paolo Soliani, and Franco Gambale
Istituto di Biofisica, Consiglio Nazionale delle Ricerche, Genoa, Italy

ABSTRACT KDC1 is a voltage-dependent *Shaker*-like potassium channel subunit cloned from *Daucus carota* which produces conductive channels in *Xenopus* oocytes only when coexpressed with other plant *Shaker* potassium subunits, such as KAT1 from *Arabidopsis thaliana*. External Zn^{2+} determines a potentiation of the current mediated by the dimeric construct KDC1-KAT1, which has been ascribed to zinc binding at a site comprising three histidines located at the S3-S4 (H161, H162) and S5-S6 (H224) linkers of KDC1. Here we demonstrate that also glutamate 164, located in close proximity of the KDC1 S4 segment, is an essential component of the zinc-binding site. On the contrary, glutamate 159, located in symmetrical position with respect to E164 in the sequence $E_{159}XHHXE_{164}$ but more distant from the voltage sensor, does not play any role in zinc binding. The effects of Zn^{2+} can be expressed as a "shift" of the gating parameters along the voltage axis. Kinetic modeling shows that Zn^{2+} slows the closing kinetics of KDC1-KAT1 without affecting the opening kinetics. Possibly, zinc affects the movement of the voltage sensor in and out of the membrane phase through electrostatic modification of a site close to the voltage sensor.

INTRODUCTION

Metal ions were early recognized to play fundamental roles in plant processes acting as cofactors in enzyme activity, osmotic regulators, and current carriers on structural functions of proteins as well as in protein-protein interaction (1). Some metals, like zinc, are essential for plant growth and development. Zinc deficiency determines reduction of young leaf growth, distortion of leaf margins, chloroses, and necrosis in leaves and delay of stem growth (2). Zinc is also involved in the modulation of the properties of channels such as the voltage-gated channels (3–5), NMDA receptor channels (6,7), GABA channels (8), and chloride channels (9). In numerous zinc-binding proteins, zinc ion is typically coordinated in tetrahedral, or distorted tetrahedral structures to negatively charged residues (carboxylates and thiolates), by charge-charge interactions, and/or to neutral dipolar residues (e.g., carbonyls and imidazoles), through orientation-dependent charge-dipole interactions (10). Consequently, amino acids involved in zinc-protein interactions are histidine, glutamate, aspartate, and cysteine (11).

KDC1, belonging to the AtKC1 family (group IV of the voltage-dependent *Shaker*-like plant K^+ channels), is an inward-rectifying potassium channel gene cloned from carrots (12). KDC1 forms heteromeric functional channels in *Xenopus laevis* oocytes when coexpressed with other inward rectifying plant potassium channels (13–15). Interestingly, currents of heteromeric channels comprising KDC1 are not inhibited (as it typically occurs for other plant channels investigated so far) (16) but, on the contrary, potentiated by the addition of zinc to the bath solution (13–15).

Alignment of amino-acid sequences of different K^+ channels revealed the presence of a unique zinc-binding site in KDC1. Specifically, KDC1 has two histidine pairs (H161 and H162) in the S3-S4 and (H224 and H225) in the S5-S6 linkers; moreover, two glutamates (E159 and E164) symmetrically flank histidines H161-H162 in the sequence: $E_{159}MH_{161}H_{162}GE_{164}$.

We already investigated the role played by histidines in Zn^{2+} potentiation of the current mediated by KDC1 coexpressed with other inward rectifying channels such as DKT1 (17) and KAT1 from *Arabidopsis thaliana* (14). We demonstrated that H224 plays a crucial role in the interaction between zinc and the channel determining current potentiation. Instead, the single mutations H161A and H162A did not significantly affect Zn^{2+} potentiation of the current; only the simultaneous mutation of both histidines determined effects comparable to those induced by H224A. We already demonstrated (13,14) that while the specific zinc-binding to extracellular histidines is responsible for current potentiation, zinc has an inhibitory effect on K^+ permeation through the homomeric KAT1 as well as the heterodimeric KDC1-KAT1 pore, owing to the binding of zinc to histidine (H267) present in the H5 segment of KAT1 (as well as all other plant inward rectifying channel) (18,19); in KDC1 this histidine is exceptionally replaced by a tyrosine in position 269.

As glutamic acids are implicated in zinc-binding domains, we decided to investigate in detail whether E159 and/or E164 participate in the site responsible for current potentiation of heteromeric channels comprising KDC1 units. To this purpose, we used a dimeric KDC1-KAT1 construct encoding a dimer where KDC1 is covalently linked to KAT1. Our study provides also indications on the biophysical mechanisms of the zinc-KDC1 interaction.

MATERIALS AND METHODS

Molecular biology

Preparation of KDC1 and KDC1-KAT1 constructs were made as previously reported (14). Mutant KDC1-KAT1 dimers were obtained by a Quikchange

Submitted June 1, 2007, and accepted for publication August 3, 2007.

Address reprint requests to Cristiana Picco, E-mail: picco@ge.ibf.cnr.it.

Editor: Toshinori Hoshi.

0006-3495/08/01/424/10 $2.00

doi: 10.1529/biophysj.107.114009

Site-Directed Mutagenesis Kit (Stratagene, La Jolla, CA). All mutations were confirmed by sequencing. Templates were linearized by *Nhe*I restriction enzyme and in vitro transcription was performed using the mCAP-RNA Capping Kit (Stratagene).

Oocyte expression and electrophysiology

Oocytes were isolated from *Xenopus laevis* females (20) and injected with cRNA (0.4 $\mu g/\mu l$) encoding for wild-type and mutated dimeric constructs using a Drummond ''Nanoject'' microinjector (50 nl/oocyte) (Drummond Scientific, Broomall, PA). Whenever a comparison was made, we performed experiments on the same batch of oocytes, from the same frog, always on the same day from the injection. Whole cell K^+ currents were measured with a two-microelectrode homemade voltage-clamp amplifier (designed by F. Conti), using 0.2–0.4 MΩ electrodes filled with 3 M KCl. The following standard bath solution was used (in mM): 100 KCl, 2 $MgCl_2$, 1 $CaCl_2$, 10 MES/Tris, pH 5.6. A quantity of 1 mM $LaCl_3$ was added to the bath solution to inhibit oocyte endogenous currents elicited by potentials more negative than −160 mV (15,21). Zn^{2+} was added to the external standard solution as $ZnCl_2$ at different concentrations. Unless otherwise indicated, experiments were performed in standard ionic solutions +1 mM $LaCl_3$.

Data analysis

The relative open probability was obtained dividing the steady-state currents by (V-V_{rev}) and normalizing to the saturation value of the calculated Boltzmann distribution. Unless otherwise indicated, experimental data points represent mean values of at least five experiments ± SE. Half-activation potentials ($V_{1/2}$) and apparent gating charge, z, were determined by fitting experimental points with a single Boltzmann isotherm of the form: $P_{open} = 1/(1 + \exp(zF(V\text{-}V_{1/2})/RT))$. Half-activation times, $t_{1/2}$, represent the time where the current reaches half of its maximum values. Deactivation time constants were evaluated by a best fit of tail currents, obtained after a main pulse to −160 mV, with a single exponential function.

The dose-response analysis of zinc potentiation was obtained by subtraction between the half-activation potential determined in the presence and in the absence of zinc ($V_{1/2}$(Zn)-$V_{1/2}$(control)) and fitted by a modified Hill equation (see text and Fig. 6).

Model for metal binding

To quantify zinc effects on potassium current we adopted the shift and scaling model described by Elinder for metal binding and modulation of ion channels (22). We use the simple two-state model and consider the basic one-site model represented in Scheme 1,

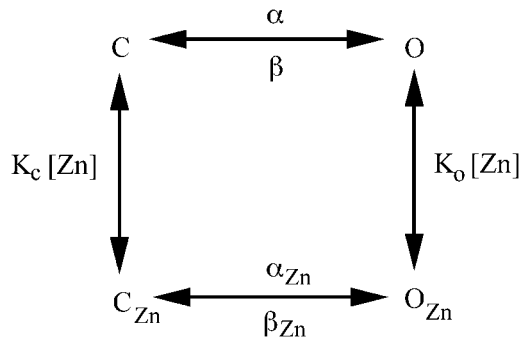

SCHEME 1

where C and O are closed and open states; K_C and K_O are the binding constants of Zn^{2+} for the closed and open states, respectively; [Zn] is the concentration of zinc ions; and α and α_{Zn}, β and β_{Zn} are the unbound or bound-metal rate constants, respectively. The voltage-dependent rate constants are expressed as

$$\alpha = k_{eq}\exp((V - V_{eq})z_\alpha FR^{-1}T^{-1}), \quad (1)$$

$$\beta = k_{eq}\exp(-(V - V_{eq})z_\beta FR^{-1}T^{-1}), \quad (2)$$

where k_{eq} is the rate constant of α and β when $\alpha = \beta$, V_{eq} the membrane voltage when $\alpha = \beta$, z_α the gating valence for α and z_β the gating valence for β, and F, R, and T the usual thermodynamic parameters. If the model is in thermodynamic equilibrium then

$$K_O = K_C a_{Zn}\beta/\alpha\beta_{Zn}. \quad (3)$$

We suppose that Zn^{2+}-binding is much faster than the channel gating, therefore the previous scheme can be reduced to

$$\{C\} \underset{\beta_{Zn}}{\overset{\alpha_{Zn}}{\longleftrightarrow}} \{O\}, \qquad \text{SCHEME 2}$$

where $\{C\}$ defines all the closed states and $\{O\}$ all the open states. The rate constants for the zinc-ion bound states can be expressed as

$$\alpha_{Zn} = \alpha(1 + K_C[Zn]\exp(-\Delta V_{Zn}z_\alpha FR^{-1}T^{-1}))/(1 + K_C[Zn]), \quad (4)$$

$$\beta_{Zn} = \beta(1 + K_C[Zn]\exp(-\Delta V_{Zn}z_\alpha FR^{-1}T^{-1}))/(1 + K_C[Zn] \times \exp((-\Delta V_{Zn}(z_\alpha + z_\beta)FR^{-1}T^{-1})), \quad (5)$$

where ΔV_{Zn} is the shift of the electrical potential induced by one bound Zn^{2+} ion. From these equations the shift of the open probability curves, $P = \alpha/(\alpha+\beta)$, versus Zn^{2+} concentration can be expressed in term of $V_{1/2}$ as

$$\Delta V_{1/2} = RT/(F(z_\alpha + z_\beta))\ln((1 + K_C[Zn])/(1 + K_C[Zn] \times \exp(-\Delta V_{Zn}(z_\alpha + z_\beta)FR^{-1}T^{-1}))). \quad (6)$$

RESULTS

We have previously shown (13–15) that both KDC1, coexpressed with KAT1 (an inward rectifying potassium channel from *Arabidopsis thaliana* (18,23)), and the dimeric construct KDC1-KAT1 display current-voltage characteristics shifted toward more hyperpolarizing membrane potentials with respect to KAT1 alone (13,14,24). This does not allow a full characterization of the current-voltage characteristics, in *Xenopus* oocytes, of heteromeric channels comprising KDC1 because, at potentials more negative than −160 mV, typical endogenous chloride currents overlap to potassium currents of heteromeric KDC1:KAT1 or dimeric KDC1-KAT1 channels. Since it has been shown that La^{3+} blocks the hyperpolarization-activated (chloride) currents (21), to eliminate the endogenous oocyte currents, we decided to add 1 mM lanthanum (as $LaCl_3$) to the standard bath solution. As demonstrated in Fig. 1, in our working conditions La^{3+} blocks endogenous oocyte currents without affecting potassium KDC1-KAT1 currents. Fig. 1 *A* shows inwardly rectifying currents activated by hyperpolarizing

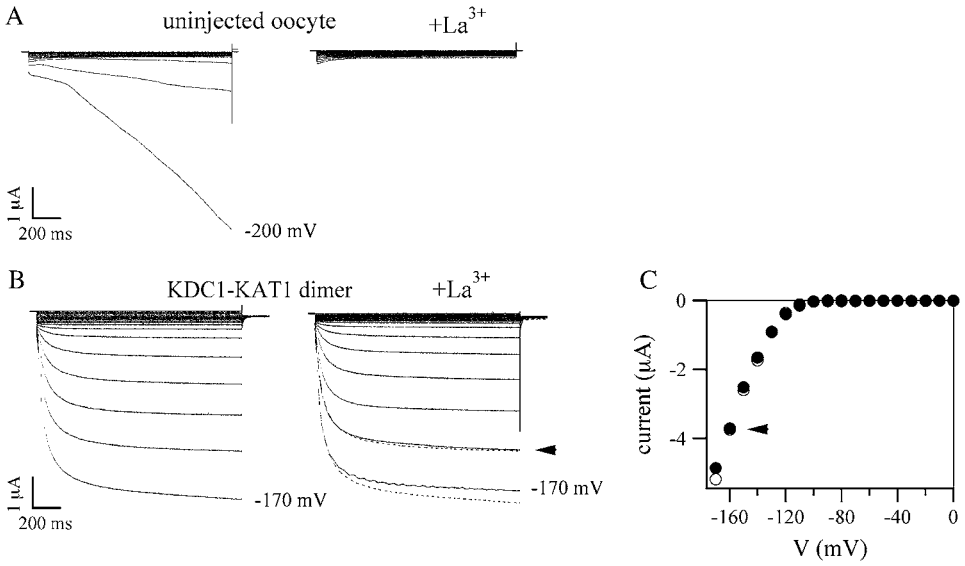

FIGURE 1 Lanthanum inhibits oocyte endogenous currents but does not affect KDC1-KAT1 currents. (*A*) Lanthanum inhibits endogenous currents in oocytes. (*Left*) Typical currents measured in an uninjected oocyte challenged with hyperpolarizing potentials from 0 mV to −200 mV in −20 mV decrements; standard bath solution. Typical endogenous hyperpolarization-activated chloride currents were observed at potentials ≤−160 mV. (*Right*) Typical currents recorded from the same oocyte after the addition of 1 mM La^{3+} to the external bath solution. La^{3+} completely inhibits the endogenous currents. (*B*) Lanthanum does not affect KDC1-KAT1 currents. Typical currents measured in an oocyte injected with the KDC1-KAT1 dimeric construct in response to voltage steps from 0 to −170 mV, in −10 mV decrements, in the absence (*left*) and in the presence (*right*) of 1 mM La^{3+}. (*On the right*) Traces measured without La^{3+} at $V = -160$ mV and $V = -170$ mV (*dotted lines*) were superimposed to traces recorded in the presence of La^{3+}. (*C*) Current-voltage characteristics of traces illustrated in panel *B*. Solid circles represent the mean value of the current during the last 50 ms of each trace in the presence of La^{3+}. Open circles represent the mean value of current, calculated as before, measured in the absence of lanthanum. Up to the current trace indicated by the arrowhead (*B*, *right*), the current-voltage characteristics were almost identical. Instead, in the absence of La^{3+}, endogenous currents, activated by voltages more negative than −160 mV, add to potassium currents changing the current-voltage characteristics.

voltage steps (up to −200 mV) applied to an uninjected oocyte in the absence (*left*) and in the presence (*right*) of lanthanum. It can be observed that endogenous currents activated by voltages more negative than −160 mV, were completely blocked by the addition of lanthanum. We challenged oocytes injected with the KDC1-KAT1 dimeric construct comparing total currents in the range where endogenous currents were not activated yet, i.e., until $V \approx -160$ mV. Fig. 1 *B* shows that K^+ currents (elicited by hyperpolarizing voltage steps up to −170 mV) in the absence and in the presence of La^{3+} were very similar. Only a slight difference at −170 mV, due to the activation of the endogenous currents, could be observed (see *current-voltage curves* in Fig. 1 *C*). These results indicate that La^{3+} did not influence the heteromeric potassium channel activity while it allowed us to apply membrane potentials as large as −240 mV. Therefore, the addition of La^{3+} allowed us to study the current voltage characteristic of KDC1-KAT1 channels in more detail.

Interestingly, zinc increases the ionic current mediated by KDC1 subunit, coexpressed with other plant K^+ channels (13). As previously shown (14,15), this property can be ascribed to histidines located between the α-helices S3-S4 and S5-S6. Since glutamic acid typically plays a relevant role in zinc coordination of proteins, involving at least three amino acids, it was worthwhile to investigate whether one or both glutamic acids (E159 and E164), symmetrically flanking the histidine pair H161 H162 in the sequence EMHHGE, participate in the zinc-binding site (14).

To fulfill this objective, E159 and E164 were individually mutated into the electrically conservative aspartic acid (i.e., E159D or E164D) or the electrically neutral amino-acid alanine (E159A or E164A) as well as the positively charged amino-acid lysine (E159K or E164K). All the single point mutations generated functionally conductive channels, displaying activation properties very similar to those of the wild-type channel. As an example, Fig. 2 displays typical heteromeric inwardly rectifying currents recorded in oocytes injected with (*A*) the wild-type dimeric construct KDC1-KAT1 and (*B*) the mutants KDC1(E159A)-KAT1 (indicated as E159A) or (*C*) KDC1(E164K)-KAT1 (indicated as E164K). Also the mutants carrying the negatively charged aspartic acid and the positively charged amino-acid lysine, in position 159 or in position 164, mediated ionic currents (not shown) with current-voltage characteristics similar to those of the wild-type (Fig. 2, *D* and *E*, respectively). Interestingly, mutation E164K, introducing a positive charge contiguous to the voltage sensor, determined the more significant shift of the activation characteristics toward more negative membrane potentials, with respect to the wild-type (see Table 1, column 7: $\delta V_{1/2} = (217.4 - 207.9) = 9.5$ mV).

On this basis, we could investigate whether the mutated channels responded to zinc in a different manner with respect to the wild-type. Fig. 3 illustrates the effect of 1 mM zinc on the wild-type and mutated dimers. Also, in this case La^{3+} did not interfere with the effect of Zn^{2+} on ionic currents (data not shown). It can be observed that no mutation of the glutamic acid in position 159 changed the zinc-sensitivity of

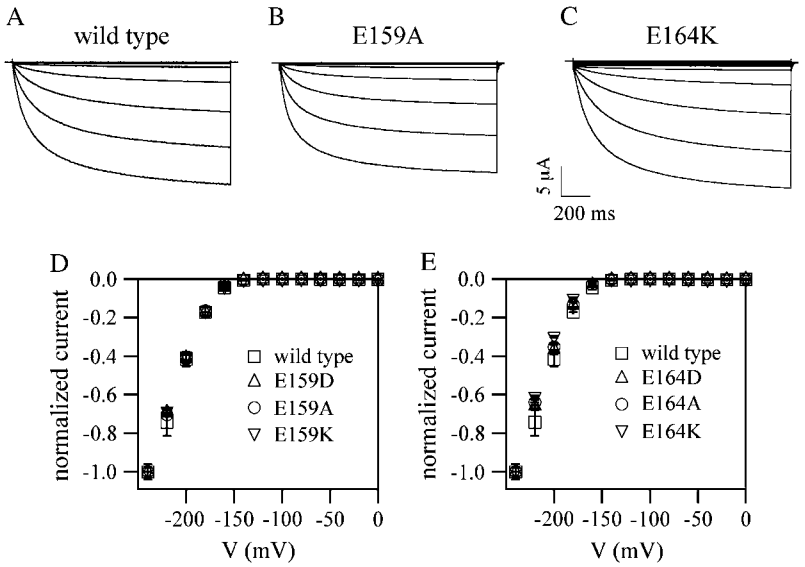

FIGURE 2 KDC1-KAT1 constructs mutated in residues E159 and E164 express functional channels. Typical inward rectifying potassium currents measured from oocytes injected with (*A*) the wild-type dimeric construct and the mutated (*B*) E159A or (*C*) E164K constructs. Applied membrane potentials from 0 mV to −240 mV in −20 mV decrements. Holding and tail potential were 0 and −50 mV, respectively. Current-voltage characteristics of wild-type and dimers mutated in (*D*) E159 and (*E*) E164. All currents were normalized to their respective maximum currents (at −240 mV). Mean values from at least five different experiments ± SE. Symbols for the wild-type and mutated channels are indicated.

the KDC1-KAT1 dimer (Fig. 3, *A* and *B*). On the contrary, mutations of E164 (Fig. 3 *C*) determined a different sensitivity to zinc depending on the characteristics of the mutated amino acid. If the charge was conserved, as in E164D, the heteromeric channel still displayed the typical potentiation of the current induced by zinc; vice versa, when the charge of glutamic acid was substituted by the positive charge of lysine or by the neutral alanine, zinc-potentiation was removed and a zinc-mediated inhibition of the current was observed. These results demonstrated that, contrary to E159, glutamate 164 is involved in zinc binding. Moreover, the electric charge of glutamate 164 seems to play a role in zinc binding as also the negatively charged aspartic acid appears to be a potential partner in zinc binding, presumably through its carboxylate group (25). Zinc effects on the current are summarized for the wild-type and the mutated channels in Fig. 3 *D*, where the steady-state currents, elicited by a voltage pulse to −160 mV in the presence of 1mM external Zn^{2+}, was compared to the currents in the absence of Zn^{2+}. It can be observed that the mutated channels, which are still potentiated by zinc, present the same current amplification of the WT channel, thus confirming that glutamate E159 does not participate in zinc binding. On the other hand, also Zn^{2+} inhibition of the mutated E164A and E164K channels was comparable (i.e., ≈20%) to the inhibition measured in the homomeric KAT1 channel and the mutated H224A and H161A-H162A heterodimeric channels (14).

Analysis of the current characteristic versus the applied potential may provide an useful tool to distinguish zinc-potentiation from zinc-inhibition and to identify the contributions of different amino acids in the two mechanisms. Interestingly, we observed a different behavior for inhibition or potentiation of the currents induced by Zn^{2+}. The inhibition of the currents appeared to be voltage-independent, in the range from −160 to −240 mV (Fig. 4 *A*), whereas Zn^{2+}-potentiation was clearly voltage-dependent (Fig. 4 *B*).

TABLE 1 Half-activation potentials and apparent gating charges for the WT and the mutated KDC1-KAT1 dimeric channels

	Control		Zinc 1 mM					
Channel	$V_{1/2}$	z	$V_{1/2}$	z	$\Delta V_{1/2}$	$\delta V_{1/2}$	$\Delta z/z$	N
WT	−207.9 ± 0.7	1.31 ± 0.04	−198.5 ± 0.8	1.16 ± 0.04	9.4		0.13	5
E164D	−212.9 ± 0.5	1.41 ± 0.04	−203.2 ± 0.7	1.36 ± 0.05	9.7	5.0	0.04	5
E164A	−209.9 ± 0.6	1.43 ± 0.04	−209.3 ± 0.6	1.39 ± 0.05	0.6	2.0	0.04	6
E164K	−217.4 ± 0.5	1.45 ± 0.04	−216.5 ± 0.5	1.43 ± 0.04	0.9	9.5	0.01	5
E159D	−204.1 ± 0.7	1.22 ± 0.05	−195.1 ± 0.8	1.14 ± 0.05	9.0	−3.8	0.07	6
E159A	−205.7 ± 0.7	1.64 ± 0.07	−196.0 ± 1.0	1.49 ± 0.08	9.7	−2.2	0.10	5
E159K	−210.4 ± 0.6	1.48 ± 0.05	−201.2 ± 0.7	1.40 ± 0.05	9.2	2.5	0.06	5

Half-activation potential, $V_{1/2}$(mV), and apparent gating charge, z, obtained by the best fit of the open probability distribution with a single Boltzmann equation, for the wild-type and mutated channels in the absence and in the presence of 1 mM Zn^{2+}; $\Delta V_{1/2}$ represents the shift of the half-activation potential and $\Delta z/z$ the relative variation of the apparent gating charge, after Zn^{2+} addition. $\delta V_{1/2}$ represents the shift of the half -activation potential of each mutant with respect to the WT in control conditions (N = number of experiments).

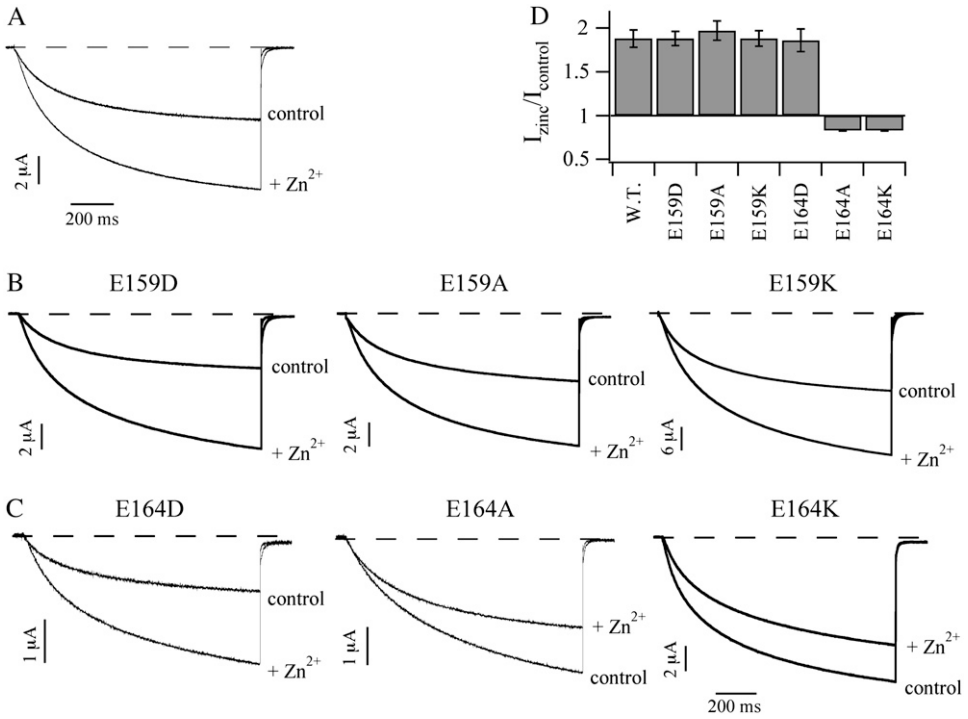

FIGURE 3 E164 is involved in zinc potentiation of the current while E159 is not. Ionic currents recorded before and after the addition of 1 mM Zn^{2+} to the bath solution from oocytes injected with WT and different mutated dimeric constructs. (*A*) Current potentiation measured in WT channel. (*B*) Current potentiation was preserved irrespective of the charge-conservative (*D*, *left panel*) or nonconservative (*A*, *center panel* and *K*, *right panel*) mutation introduced in E159. (*C*) From left to right, the conservative mutation E164D also preserved current potentiation while the nonconservative mutations (E164A and E164K) abolished current potentiation. Holding, step, and tail potentials were 0 mV, −160 mV, and −50 mV, respectively. (*D*) Percentage of current change induced by 1 mM Zn^{2+} measured at $V = -160$ mV for the wild-type and mutated dimeric channels. Mean values from at least eight different experiments ± SE.

Currents potentiation decreased with the increase of hyperpolarizing membrane potentials; at potentials more negative than −200 mV, the currents were no longer enhanced by the addition of Zn^{2+}.

Further information on zinc-mediated current-potentiation was obtained from open probability curves. As shown in Fig. 5, zinc shifted the Boltzmann curves toward more depolarizing membrane potentials with respect to control solution (absence of zinc) both for the wild-type channel (Fig. 5 *A*) and the mutated channels E159D (Fig. 5 *B*), E159A (Fig. 5 *C*), and E159K (Fig. 5 *D*) as well as E164D (Fig. 5 *E*). On the contrary, when residue E164 was mutated into a neutral or positive residue, the shift was removed and the two normalized Boltzmann curves (in the presence and in the absence of zinc) superimposed (Fig. 5, *F* and *G*, respectively). Therefore, current potentiation is clearly due to a shift of the normalized conductance toward less hyperpolarizing membrane potentials. The amplitude of the voltage shift was very similar for the wild-type and all the conservative mutations of the channel as summarized in Fig. 5 *H* and in Table 1. Moreover, no appreciable differences of the apparent gating charges were observed between the wild-type and the mutated channels (Fig. 5 and Table 1).

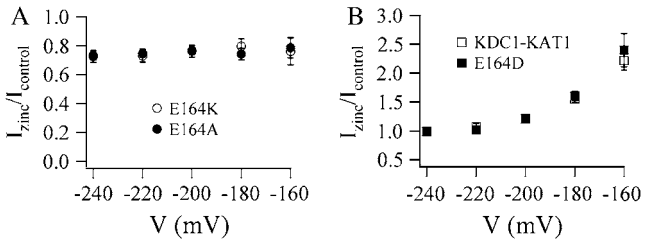

FIGURE 4 Current potentiation mediated by zinc is voltage-dependent, whereas current inhibition is voltage-independent. (*A*) The current decrease induced by 1 mM Zn^{2+} normalized to the control ($I_{zinc}/I_{control}$) in the mutated dimeric channels E164A and E164K was plotted versus the potential. (*B*) The normalized current increase induced by 1 mM Zn^{2+}, in the wild-type dimer and the mutated E164D dimer. Values (± SE) represent the mean of at least five experiments.

To estimate Zn^{2+} affinity for the KDC1-KAT1 channel, the voltage dependence of activation was determined at different Zn^{2+} concentrations (Fig. 6 *A*). Increasing the Zn^{2+} concentration from 0.1 to 5 mM resulted in a progressive shift of the open probability curve toward the positive direction. The curves at different concentrations were fitted with the Boltzmann function to obtain the half-activation potential, $V_{1/2}$. The difference in $V_{1/2}$ ($\Delta V_{1/2}$) in the presence and in absence of zinc, determined from the curves in Fig. 6 *A*, was plotted versus the logarithm of Zn^{2+} concentration (Fig. 6 *B*, *left axes*).

Data in Fig. 6 *B*, fitted by the Hill equation

$$\Delta V_{1/2} = \Delta V_{max}([Zn]/K_d)^n/(1 + ([Zn])/K_d)^n),$$

where ΔV_{max} (the saturation value of the voltage shift), n (the Hill coefficient), and K_D (the Zn^{2+} concentration for the half-maximal voltage shift) gave the following values: $\Delta V_{max} =$ 15.5 mV, $K_D = 387$ μM, and $n = 0.9$. Similar results were obtained from others experiments and gave the mean values: $\Delta V_{max} = 13 \pm 1$ mV, $K_D = 376 \pm 137$ μM, and $n = 0.7 \pm 0.2$

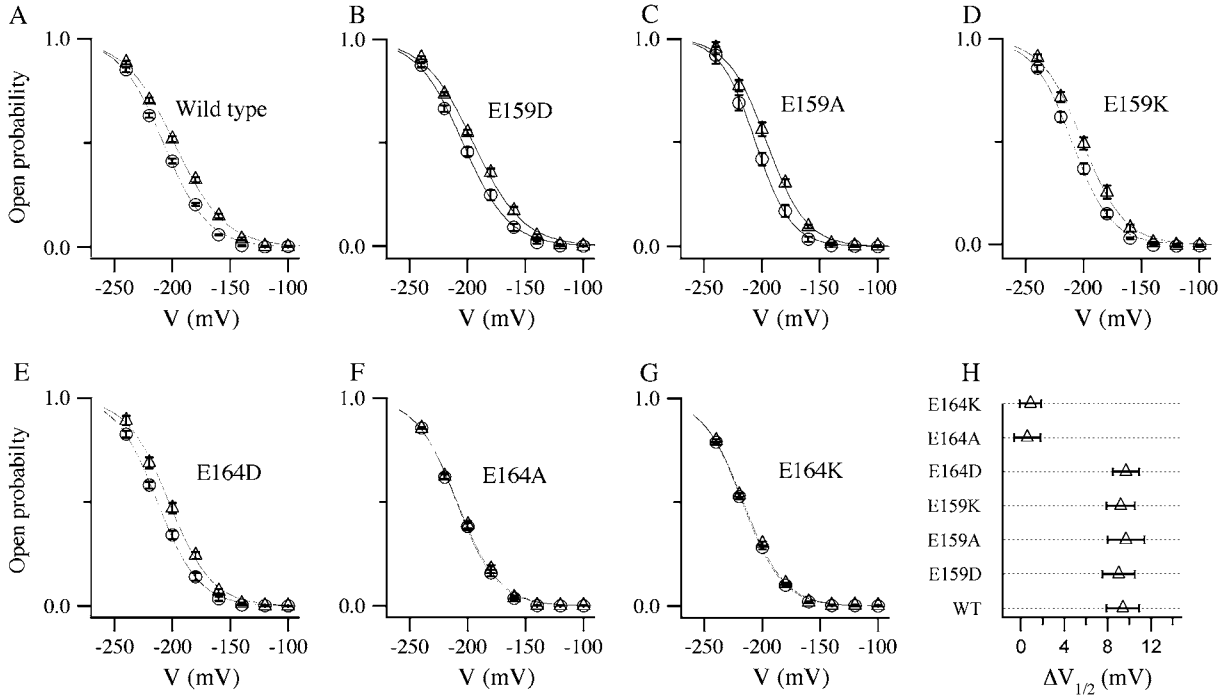

FIGURE 5 Voltage shift of the open probability in the WT and mutated channels. Open probability curves in the absence (*open circles*) and in the presence (*open triangles*) of 1 mM $ZnCl_2$ for the wild-type dimeric construct (*A*) and for the dimeric constructs mutated as follows: (*B*) E159D, (*C*) E159A, (*D*) E159K, (*E*) E164D, (*F*) E164A, and (*G*) E164K. When E164 was mutated to an electrically nonconservative residue as alanine or lysine, the open probabilities in the absence and presence of zinc were undistinguishable. Continuous lines are the best fits of experimental data with the Boltzmann equation (mean values ± SE, $N \geq 5$). (*H*) Differences in $V_{1/2}$ ($\Delta V_{1/2}$) obtained in the presence and in the absence of zinc for the wild-type and the mutated dimeric constructs (mean values ± SE, $N \geq 5$) (see also Table 1). The shifts of the activation voltage, induced by 1 mM Zn^{2+}, were identical, within experimental error, for the WT and the mutated channels displaying zinc potentiation.

($N = 5$). Zn^{2+} affinity estimated from the best fit of the normalized current ($I_{zinc}/I_{control}$ in Fig. 6 *B*, *right axes*) with the Hill equation gave comparable K_D and n values at $V = -160$ mV, i.e.: $K_D = 401$ and $n = 0.9$.

To investigate the mechanism of zinc potentiation mediated by KDC1, we analyzed the activation and deactivation parameters and the shift induced by zinc in these curves. The measurements used for ON and OFF kinetics were the half-time of activation ($t_{1/2}$) and deactivation time constant (τ). Fig. 7 *A* shows the action of 1 mM Zn^{2+} on activation kinetics. The two traces, recorded from the same oocyte, challenged by voltages hyperpolarizing the cell to −160 mV, in the presence and in the absence of zinc (Zn^{2+} trace has been scaled to match the steady value of the trace in control), are nearly indistinguishable. On the contrary, Zn^{2+} slowed the closing kinetics of the channel (Fig. 7 *B*). To evaluate the voltage shift dependence of current kinetics induced by zinc, the mean values of $t_{1/2}$ (Fig. 7 *C*) and τ (Fig. 7 *D*) were plotted versus the applied voltage. Consistently with typical currents obtained at $V = -160$ mV, zinc did not affect the activation kinetic at all potentials, whereas it slowed down the deactivation kinetics.

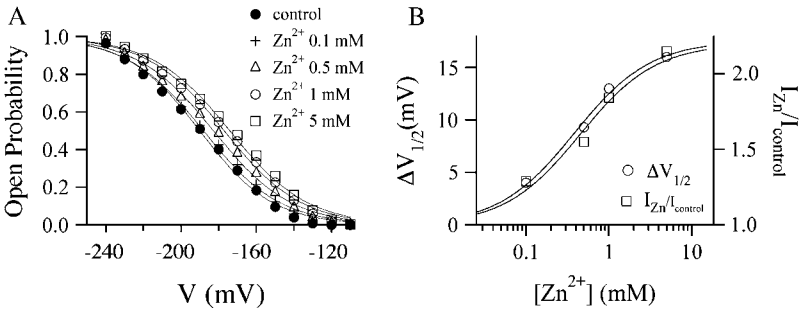

FIGURE 6 Open probability shift depends on Zn^{2+} concentration. (*A*) Open probability curves in the absence and in the presence of different Zn^{2+} concentrations in the bath solution plotted as a function of the membrane potential for the WT KDC1-KAT1 channel (*symbols* in control solution and for each Zn^{2+} concentration are indicated in the figure). Continuous lines are the best fits of experimental data with the Boltzmann equation. (*B*) Semilogarithmic plot of the half-activation potentials (*open circles*) derived from the best fit of the data in panel *A* and of $I_{zinc}/I_{control}$ (*open squares*) at $V = -160$ mV versus Zn^{2+} concentration. Both data were fitted with the Hill equation.

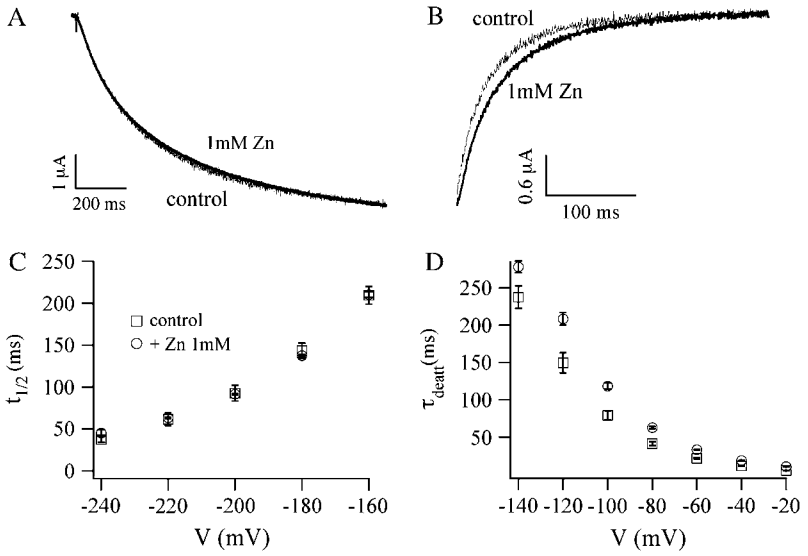

FIGURE 7 Effects of Zn^{2+} on the activation and deactivation kinetics of the KDC1-KAT1 channel. (*A*) Typical kinetics of activation of the WT KDC1-KAT1 current recorded at −160 mV in control solution and in the presence of 1 mM Zn^{2+}. The trace in the presence of Zn^{2+} has been scaled to match the steady value of the trace in control conditions. Traces are nearly undistinguishable. (*B*) Typical kinetics of deactivation currents recorded at −80 mV, before and during Zn^{2+} application. Data were obtained from the same oocyte investigated in panel *A*. (*C*) Half-times of current activation, $t_{1/2}$, before (*open squares*) and during (*open circles*) Zn^{2+} application, plotted versus membrane potential. (*D*) Time constants of currents deactivation, τ, calculated in the presence and in the absence of Zn^{2+}, plotted versus membrane potential. Same symbols as in panel *C*. Mean values from at least five different experiments ± SE.

DISCUSSION

In this work, our aim was to provide more information on the amino acids participating in the zinc-binding site and on the biophysical basis for zinc sensitivity of heteromeric plant channels comprising KDC1 subunits. We demonstrated that, in addition to histidines 161, 162, and 224 (as shown in (14)), glutamate 164, also located in the KDC1 S3-S4 linker, is involved in the potentiation of potassium currents induced by extracellular zinc.

Zinc shifts the open probability curves of the KDC1-KAT1 channel

KDC1-KAT1 channels mutated in histidine H224 or in H161A-H162A of KDC1 (14) did not display Zn-potentiation but were slightly inhibited by Zn^{2+}, as observed for KAT1 and other plant *Shaker* channels (13,26). These observations confirm that Zn^{2+}, beside interacting with the KDC1 external binding site, presumably also interacts with a second lower affinity (≈10 mM) site which was previously identified with the KAT1 histidine H267 located in the external part of the pore segment (13,14). Indeed, it has already been demonstrated that mutations in the pore histidine of inward rectifying plant channels reduce zinc inhibition (see (13) and (26)).

Similarly, also heterodimeric KDC1-KAT1 channels where E164 was mutated into a nonconservative amino acid (i.e., E164A or E164K), displayed a moderate decrease of the current induced by Zn^{2+} comparable (i.e., between 20% and 30%) to the inhibition observed on the homomeric KAT1 channel (14).

The block of the endogenous currents by external La^{3+} gave us the opportunity to investigate the voltage dependence of zinc action up to very negative membrane potentials and to determine that channel inhibition and channel potentiation are regulated by voltage-independent and voltage-dependent mechanisms, respectively. Voltage-independent channel inhibition induced by zinc, observed also in KAT1 channel ((13)), is consistent with the location of H267 outside the narrowest voltage-sensitive region of the selectivity filter (27). These characteristics represent typical fingerprinting of the two mechanisms and help to monitor which one of them is preserved or abolished in the different mutants. Previous results from single-channel recordings (14) demonstrated that zinc did not affect the single-channel amplitude, while the half-activation potential apparently remained almost unaltered. This was probably due to the fact that in the absence of La^{3+}, it was not possible to apply large hyperpolarizing membrane potentials and therefore the open probability curves of KDC1-KAT1 heterodimers hardly reached a saturation value. Instead, in this article, abolition of endogenous currents allowed us to definitely state that zinc shifts the open probability of the channel toward more positive membrane potentials. As a consequence, potentiation is larger at low values of the Boltzmann distribution, decreasing when the curve reaches saturation, i.e., when the open probability reaches its maximum values. Indeed, at negative potentials of −160 mV, zinc potentiation was larger (current increased ≈2–3 times) while at more negative voltages the current increase was drastically reduced and even abolished at extremely negative membrane potentials ($I_{zinc}/I_{control}$ being ≈1 at $V = -240$ mV) (Fig. 4 *B*).

The comparable current-decrease and the absence of any voltage-dependency in the current inhibition of the homomeric KAT1 channel and heteromeric channels mutated in the external zinc-binding amino acids, suggest that appropriate (for example, nonconservative) modifications of the

external binding site completely remove zinc potentiation without affecting zinc inhibition.

Mechanism of current potentiation mediated by zinc

Metal ions can affect ion channels either by blocking the current or by modifying the gating. The effects on the gating of voltage-gated channels can be described by modifications of the voltage-dependent parameters, and can be ascribed to three main mechanisms (22). The first mechanism assumes electrostatic screening of fixed charges and predicts equal shifts of all voltage-dependent parameters. The second mechanism assumes metal binding and consequent electrostatic effects on the voltage sensor. The third and last mechanism assumes binding and accompanying nonelectrostatic effects on the gating; this might either directly affect the voltage sensor or other parts of the gating mechanism. Occasionally, a single mechanism cannot explain the results induced by some metals such as the lanthanides as well as Zn^{2+}; in these cases, it is necessary to hypothesize combined mechanical and electrostatic actions of mechanisms 2 and 3.

Our results suggest that zinc interaction with KDC1 is not due to a simple screening of surface charges: indeed, the shifts of the voltage parameters $\tau(V)$ and $P_{open}(V)$ are not identical. The shift induced by 1 mM zinc on $P_{open}(V)$ of the KDC1-KAT1 channel is ~10 mV, i.e., significantly different from that of the activation and the deactivation times. In particular, 1 mM Zn^{2+} leaves the time for half-activation practically unaffected while it slows down the deactivation time constant (by 15–20 mV).

Investigating depolarization-activated potassium channels, Gilly and Armstrong (28) found that Zn^{2+} slowed down the channel opening leaving the closing rates almost unaffected. They suggested that Zn^{2+} has a higher affinity for the closed channel, since in this state, the voltage sensor is retracted into the channel and therefore negative membrane surface charges may participate in attracting zinc ions. Vice versa in the open-state, zinc-binding is prevented by the outside movement of the voltage sensor that pushes away metal ions by electrostatic repulsion.

It has been suggested that hyperpolarization-activated channels display a different coupling between the voltage sensor and the activation gate with respect to depolarization-activated potassium channels, i.e., during the opening the S4 segment moves from outside the membrane to inside (29). Also, experiments performed on hyperpolarization-activated KAT1 channel suggested a similar voltage movement and coupling (30).

On the basis of these considerations, we propose a molecular model for zinc binding to KDC1, similar to the electrostatic model proposed by Gilly and Armstrong, but adapted to the different coupling mechanism hypothesized for inwardly rectifying K^+ channels (Fig. 8). When the channel is open, the extraplasmatic part of the S4 segment is inside the membrane; consequently, the negative surface charges of the membrane may contribute to attract zinc ions. This favors Zn^{2+} binding to histidines and glutamate 164, stabilizing the channel in the open state. Conversely, when the channel closes, Zn^{2+} binding to the channel decreases because the total zinc concentration close to E164 is lower, and/or the structure of the binding site is modified. In a similar manner, H224 (which is presumably located in close proximity of the membrane surface) also plays a major role in zinc binding, with respect to the more distantly located histidine 225 (14).

The change in zinc affinity (for open versus closed state) has been explained by Elinder and Arhem (22) by a simple electrostatic mechanism, in which the binding of a metal ion close to the voltage sensor is state-dependent and affects the

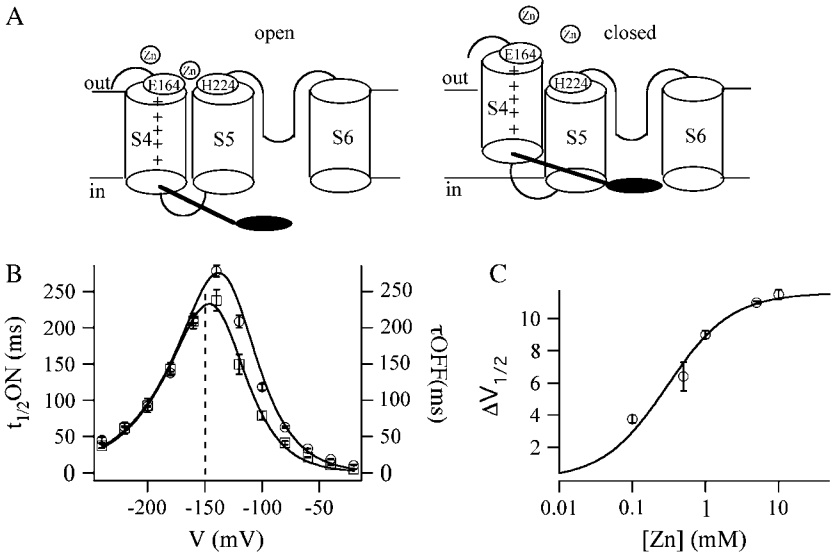

FIGURE 8 Schematic representation for Zn^{2+} binding to KDC1 and consequences on gating parameters. (*A*) A simplified model for the interaction of Zn^{2+} with the Zn^{2+}-binding site in KDC1. For simplicity reasons only the S4, S5, and S6 segments and amino acids involved in the Zn^{2+}-binding site are shown. (*B*) Plot of the time constants (separated by a *dotted line*) of activation ($t_{1/2}$, *left-hand ordinate*) and deactivation (τ, *right-hand ordinate*), of WT KDC1-KAT1 dimeric channel before (*open squares*) and during (*open circles*) Zn^{2+} application. Data are the mean of at least five experiments and were fitted by combining Eqs. 4 and 5 derived from the shift model (see Materials and Methods). The best fit to the data gave $V_{eq} = -138$ mV, $\Delta V_{Zn} = 11.6$ mV, $z_\alpha = 1.04$, $z_\beta = 0.62$, and $K_c = 4.6$ mM^{-1}. (*C*) Semilogarithmic dose-response curves of $\Delta V_{1/2}$; mean values obtained from the experimental data were fitted with Eq. 6 of the electrostatical shift model with the same values of the parameters used in panel *B*.

activation and deactivation time constants differently. Our results lead us to adopt the model proposed by Elinder and Arhem (see Materials and Methods), where the binding of a metal ion to fixed charges electrostatically modulates the voltage sensor (mechanism 2) determining a shift of gating parameters with respect to unbound control conditions. In particular, the time constants ($1/(\alpha + \beta)$), in the presence and in the absence of zinc, were fitted by combining Eqs. 4 and 5 and the results are shown in Fig. 8 *B* (see the figure legend for numerical details). Interestingly, the values found from the best fit of the data were used in Eq. 6 to fit the shifts of $V_{1/2}$ for different concentrations of zinc. Therefore a simple binding and electrostatic model is sufficient to give a reliable interpretation of the effects induced by zinc ions that are presumably mediated by a modification of an electric charge close to the voltage sensor; however, they do not directly modify the apparent gating charge of the channel (see Table 1).

The zinc-binding site

Zinc binding to proteins is frequently investigated as many proteins carry a high affinity binding site for this ion. There are now nearly 200 three-dimensional structures for zinc binding to proteins, distributed within three primary types of zinc binding sites: structural, catalytic, and cocatalytic (10). These structures provide references for the nature of zinc sites in other proteins for which only the primary structure is known. In proteins, the coordination number 4 is most common, where the zinc ion is typically coordinated in a tetrahedral or distorted tetrahedral fashion. In these sites, one zinc ion is coordinated to three amino-acid residues (histidine, glutamate and/or aspartate) and a water molecule (catalytic), or to four amino acids (mainly cysteine, but also histidine, glutamate and/or aspartate) (structural).

In the zinc-binding site of KDC1, we have identified by now at least three amino acids. Histidine 224 and glutamate 164 participate to the zinc-binding site together with histidines 161 and 162 which possibly substitute each other, while E159 and H225 are not involved in zinc binding. However, we cannot exclude that in our case, beside the amino acids listed above, some other amino acid may be involved in zinc binding.

It is worth noting here that zinc binding might be affected by a series of different parameters such as histidine protonation at acidic pH, or the constraints determined by the water-membrane interface which presumably inhibits some movements or rearrangements of the H224 and E164 residues. Finally, zinc binding in close proximity of the S3-S4 and S5-S6 linkers might result a useful tool and molecular marker providing information not only on the participation of KDC1 in heteromeric channels but also, for example, on mobility of the S4 segment as well as on possible interactions of the voltage sensor with other segments, such as the S5 segment as already shown for other inward rectifying plant channels (31).

We acknowledge the contribution of J. Scholz-Starke, who read the manuscript with a critical approach.

We acknowledge the financial support of project No. FIRB RBAUO183A9.

REFERENCES

1. Kraemer, U., and S. Clemens. 2005. Functions and homeostasis of zinc, copper, and nickel in plant. *Topics Curr. Gen.* 14:216–271.
2. Marschner, H. 1995. Mineral Nutrition of Higher Plants. Academic Press, London.
3. Bixby, K. A., M. H. Nanao, N. V. Shen, A. Kreusch, H. Bellamy, P. J. Pfaffinger, and S. Choe. 1999. Zn^{2+}-binding and molecular determinants of tetramerization in voltage-gated K^+ channels. *Nat. Struct. Biol.* 6:38–43.
4. Anumonwo, J. M., J. Horta, M. Delmar, S. M. Taffet, and J. Jalife. 1999. Proton and zinc effects on HERG currents. *Biophys. J.* 77:282–298.
5. Wang, G., C. Strang, P. J. Pfaffinger, and M. Covarrubias. 2007. Zn^{2+}-dependent redox switch in the intracellular T1–T1 interface of a Kv channel. *J. Biol. Chem.* 282:13637–13647.
6. Hatton, C. J., and P. Paoletti. 2005. Modulation of triheteromeric NMDA receptors by N-terminal domain ligands. *Neuron.* 46:261–274.
7. Rachline, J., F. Perin-Dureau, A. Le Goff, J. Neyton, and P. Paoletti. 2005. The micromolar zinc-binding domain on the NMDA receptor subunit NR2B. *J. Neurosci.* 25:308–317.
8. Wooltorton, J. R., B. J. McDonald, S. J. Moss, and T. G. Smart. 1997. Identification of a Zn^{2+} binding site on the murine GABAA receptor complex: dependence on the second transmembrane domain of beta subunits. *J. Physiol.* 505:633–640.
9. Chen, T. Y. 1998. Extracellular zinc ion inhibits ClC-0 chloride channels by facilitating slow gating. *J. Gen. Physiol.* 112:715–726.
10. Vallee, B. L., and K. H. Falchuck. 1993. The biochemical basis of zinc physiology. *Physiol. Rev.* 73:79–118.
11. Christianson, D. W. 1991. Structural biology of zinc. *Adv. Protein Chem.* 42:281–355.
12. Downey, P., I. Szabò, N. Ivashikina, A. Negro, F. Guzzo, P. Ache, R. Hedrich, M. Terzi, and F. Lo Schiavo. 2000. Kdc1 a novel carrot root hair K^+ channel: cloning, characterization and expression in mammalian cells. *J. Biol. Chem.* 275:39420–39426.
13. Paganetto, A., M. Bregante, P. Downey, F. Lo Schiavo, S. Hoth, R. Hedrich, and F. Gambale. 2001. A novel K^+ channel expressed in carrot roots with a low susceptibility toward metal ions. *J. Bioeng. Biomembr.* 33:63–71.
14. Picco, C., M. Bregante, A. Naso, P. Gavazzo, A. Costa, E. Formentin, P. Downey, F. Lo Schiavo, and F. Gambale. 2004. Histidines are responsible for zinc potentiation of the current in KDC1 carrot channels. *Biophys. J.* 86:224–234.
15. Naso, A., R. Montisci, F. Gambale, and C. Picco. 2006. Stoichiometry studies reveal functional properties of KDC1 in plant *Shaker* potassium channels. *Biophys. J.* 91:1–11.
16. Hoth, S., and R. Hedrich. 1999. Distinct molecular bases for pH sensitivity of the guard cell K^+ channels KST1 and KAT1. *J. Biol. Chem.* 274:11599–11603.
17. Formentin, E., S. Varotto, A. Costa, P. Downey, M. Bregante, A. Naso, C. Picco, F. Gambale, and F. Lo Schiavo. 2004. DKT1, a novel K^+ channel from carrot, forms functional heteromeric channels with KDC1. *FEBS Lett.* 573:61–67.
18. Anderson, J. A., S. S. Huprikar, L. V. Kochian, W. J. Lucas, and R. F. Gaber. 1992. Functional expression of a probable *Arabidopsis thaliana* potassium channel in *Saccharomyces cerevisiae*. *Proc. Natl. Acad. Sci. USA.* 89:3736–3740.
19. Becker, D., I. Dreyer, S. Hoth, J. D. Reid, H. Busch, M. Lehnen, K. Palme, and R. Hedrich. 1996. Changes in voltage activation, Cs^+

sensitivity, and ion permeability in H5 mutants of the plant K^+ channel KAT1. *Proc. Natl. Acad. Sci. USA.* 93:8123–8128.

20. Hedrich, R., M. Bregante, I. Dreyer, and F. Gambale. 1995. The voltage-dependent potassium uptake channel of corn coleoptiles has permeation properties different from other K^+ channels. *Planta.* 197:193–199.
21. Tokimasa, T., and R. A. North. 1996. Effects of barium, lanthanum and gadolinium on endogenous chloride and potassium currents in *Xenopus* oocytes. *J. Physiol.* 496:677–686.
22. Elinder, F., and P. Arhem. 2004. Metal ion effects on ion channel gating. *Q. Rev. Biophys.* 36:373–427.
23. Schachtman, D. P., J. I. Schroeder, W. J. Lucas, J. A. Anderson, and R. F. Gaber. 1992. Expression of an inward-rectifying potassium channel by the *Arabidopsis* KAT1 cDNA. *Science.* 258:1654–1658.
24. Naso, A., R. Montisci, F. Gambale, and C. Picco. 2006. Stoichiometry studies reveal functional properties of KDC1 in plant *Shaker* potassium channels. *Biophys. J.* 91:3673–3683.
25. Auld, D. S. 2001. Zinc coordination sphere in biochemical zinc sites. *Biometals.* 14:271–313.
26. Hoth, S., and R. Hedrich. 1999. Susceptibility of the guard cell K^+ uptake channel KST1 towards Zn^{2+} requires histidine residues in the S3–S4 linker and in the channel pore. *Planta.* 209:543–546.
27. Jiang, Y., A. Lee, J. Chen, M. Cadene, B. T. Chait, and R. MacKinnon. 2002. Crystal structure and mechanism of a calcium-gated potassium channel. *Nature.* 417:515–522.
28. Gilly, W. M. F., and C. M. Armstrong. 1982. Divalent cations and the activation kinetics of potassium channels in squid axon. *J. Gen. Physiol.* 79:965–996.
29. Mannikko, R., F. Elinder, and H. P. Larsson. 2002. Voltage-sensing mechanism is conserved among ion channels gated by opposite voltages. *Nature.* 419:837–841.
30. Latorre, R., R. Olcese, C. Basso, C. Gonzalez, F. Munoz, D. Cosmelli, and O. Alvarez. 2003. Molecular coupling between voltage sensor and pore opening in the *Arabidopsis* inward rectifier K^+ channel KAT1. *J. Gen. Physiol.* 122:459–469.
31. Lai, H. C., M. Grabe, Y. N. Jan, and L. Y. Jan. 2005. The S4 voltage sensor packs against the pore domain in the KAT1 voltage-gated potassium channel. *Neuron.* 47:395–406.